Journal of Ceramic Processing Research. Vol. 21, No. 2, pp. 200~207 (2020)
(Received 10 October 2019, Received in revised form 8 January 2020, Accepted 17 January 2020)
https://doi.org/10.36410/jcpr.2020.21.2.200

J O U R N A L O F
Ceramic Processing Research

Mechanism of stopping crack propagation in continuous fiber reinforced self-healing ceramic

Jang-Won Lee[a], Ki-woo Nam[b] and Wataru Nakao[a,*]
[a]*Faculty of Engineering, Yokohama National University, 79-5, Tokiwadai, Hodogaya-ku, Yokohama 240-8501, Japan*
[b]*Department of Materials Science and Engineering, Pukyong National University, 45 Yongso-ro, Nam-gu, Busan 48547, Korea*

The self-healing fiber-reinforced composite (abbreviation: shFRC) was made by adding SiC, a self-healing material, between an Al_2O_3 matrix and an Al_2O_3 continuous fiber. shFRC has the characteristic of healing the reduced strength by self-healing. The purpose of this study was to evaluate the damage and healing of new composite material, shFRC, and define new failure criteria. The test method used in this study was a high temperature creep test. The interface fracture behavior with time was investigated by analyzing the creep rate. The creep test conditions were 137 MPa and 150 MPa at 1,000 °C, and 68.5 MPa, 100 MPa, and 137 MPa at 1,200 °C, respectively. As a result, the crack propagation of 1,000 °C was stopped by healing, and the creep rate was zero. The crack healing part was higher than the strength before the crack formation. Due to the rapid hardening of the interface and the decrease in strength of the fiber, delayed fracture behavior was not observed at 1,200 °C. If the crack is stopped by self-healing at a constant load, shFRC can use that load stress as the allowable stress. However, when the reaction rate of the interface is markedly rapid, crack propagation is difficult to control.

Keywords: Damage and healing behavior, self-healing, Fiber reinforced ceramics, Crack branching, Creep test, Crack suppression.

Introduction

Ceramics have higher heat resistance and specific strength than metals. If the nickel alloy, used in the turbine blades of an aircraft jet engine, is replaced with ceramic, fuel efficiency would be dramatically increased by non-cooling and weight reduction. Improved fuel economy has the advantage in that CO_2 gas emissions are reduced, and the acceleration of global warming can be alleviated. However, their safety is significantly lower in actual operating environments because ceramics are brittle. Thus, it is not suitable as a component for an aircraft requiring high reliability. Continuous Fiber Reinforced Ceramic Matrix Composites (abbreviation: CFCC), represented by ceramic composite materials, is attracting attention as a countermeasure to compensate for these problems [1-4]. CFCC has the property in that fiber absorbs energy when a crack propagates and induces delayed fracture [5-6]. However, there is high risk of a sharp decline in strength after cracking. As a solution to this problem, we propose a method of adding self-healing to CFCC.

The healing effects of fiber reinforced composites with self-healing have already been reported in various fields. Ultra-high-performance fiber reinforced concrete (UHPFRC) have been reported to recover most of the compressive strength damaged by air and hydration reaction [7], and hollow fiber-reinforced polymer composites have been reported to recover most of the bending strength lowered by UV reaction [8]. In addition, it has been reported that the mechanical and lifetime models of self-healing ceramic matrix composites are presented, and that the coupling of mechanical and physicochemical mechanisms should be considered as a key element for predicting self-healing behavior in oxidizing environment [9]. However, no experimental cases of self-healing fiber-reinforced composite ceramics have been reported.

The interface control of CFCC plays a key role because the bond strength between the fiber and matrix has a major influence on the fracture strength and behavior [10, 11]. CFCC composite material in which self-healing material is added to the interface layer facilitates interface control by oxidation as well as heals the cracks, thereby restoring the strength weakened after the cracking to better than the strength before cracking. This new composite material is called self-healing Fiber Reinforced Ceramics (shFRC). Since shFRC is designed with the weakest part interface layer, cracks propagate along the interface layer and healing is manifested by high temperatures after crack propagation.

The purpose of this study was to secure the high reliability required at the operating environment by evaluating the fracture and healing behavior and to establish a new fracture standard for shFRC when damage and recovery occur simultaneously at high temperatures. High temperature creep tests were performed

*Corresponding author:
Tel : +81-45-339-4016
Fax: +81-45-339-4016
E-mail: Nakao-wataru-hy@ynu.ac.jp

to simultaneously produce damage (load) and healing (high temperature). Spinel-structured γ-phase alumina fibers with high heat resistance, high chemical stability, and low cost were used. And the α-phase alumina, which can maintain high strength for a lengthy duration at high temperature and has excellent chemical stability, was used as a matrix [12, 13]. SiC, known for its strength recovery by high temperature oxidation, was used as the interface layer between the matrix and fiber [14-17].

Test Methods

Specimen

The test specimen is an Al_2O_{3f}/SiC/Al_2O_3 composite containing non-oxide SiC in the interface layer of the fiber/matrix. Continuous fibers (S-640D, γ-phase, Nitivy Co., Ltd., Tokyo, Japan) use bundles of twisted bundles of approximately 640 fibers with a fiber diameter of 7 μm, and the composition is Al_2O_3 72%, SiO_2 28%. As the matrix (AKP-50, α-phase, Sumitomo Chemical Co., Ltd., Tokyo, Japan, Purity over 99.99%), an Al_2O_3 powder having an average particle diameter of 0.23 μm is used. The powder used for the interface layer is SiC (Ultrafine grade, β-phase, Ibiden Co., Ltd., Gifu, Japan, Purity over 98%) having an average particle diameter of approximately 0.35 μm. The manufacture method used filament winding method to easily control the thickness of the interface layer and the matrix. The slurry was mixed with each powder (Al_2O_3, SiC) with distilled water, a dispersant (Ammonium poly acrylate, A-30SL, TOAGOSEI CO., LTD., Japan) and a binder (Acrylic emulsion, #7110, SEKISUI CHEMICAL CO., LTD., Japan) was added and ball milled for 24 h to complete. Al_2O_3 continuous fibers were impregnated into the Al_2O_3 slurry, and then coated by passing through the drying furnace with 850 rpm at 90 °C, and the sample was obtained by repeating the filament winding process three times under the same conditions. The obtained sample was impregnated on the SiC slurry by the same methods above with 650 rpm. Sample coated up to SiC was impregnated in Al_2O_3 slurry and forming on the 60 mm × 60 mm wide plates without drying. The formed specimen was dried for 48 h at a pressure of 5 MPa. the obtained forming was heated at 300 ºC for five hours to remove dispersant and binder, and then sintered at 1300 ºC for 10 h. Sintering atmosphere is Ar. The size of the processed specimen is 8.00 mm × 50.00 mm × 1.65 mm and the diameter of the center hole is 4 mm. The interface layer is designed to be the weakest part. The thickness of the interface layer coated on the fiber is approximately 14 μm and the spacing between the fiber bundles is about 300 μm. The average diameter of the fiber bundles is 200 μm. And the average density of the specimen is 2.3 g/cm^3. The test specimen contains approximately 60 Vol.% of fiber, 9 Vol.% of interfacial layer, and 31 Vol.% of parent metal. Also, fiber orientation is one axis. Fig. 2 shows the internal structure of the completed test specimen.

Experimental set-up

When the ratio 2ρ/2b of the diameter of the hole to the width of the specimen is less than 0.5, the Howland method is regarded as highly accurate [18]. Since 2ρ/2b is 0.5 in the specimen, the stress concentration coefficient was calculated using Equation (1) proposed by Howland.

$$\alpha = 2 + \left(\frac{b-\rho}{b}\right)^3 \tag{1}$$

Wherein ρ (mm) is the radius of the hole, b (mm) is half the width of the specimen, and α is the stress

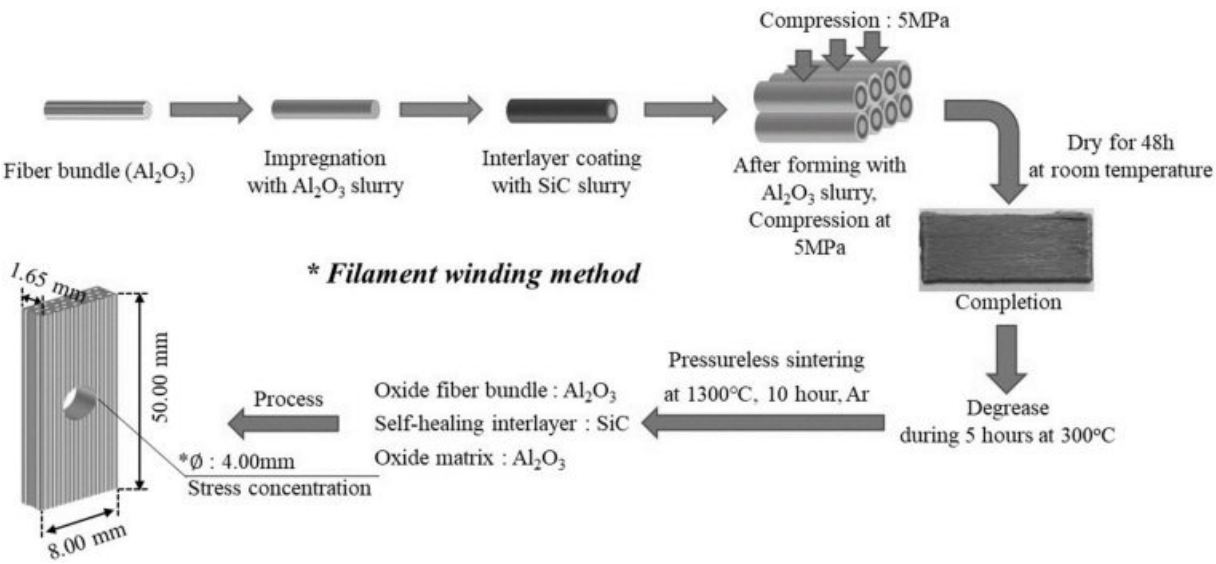

Fig. 1. The manufacturing process of specimen.

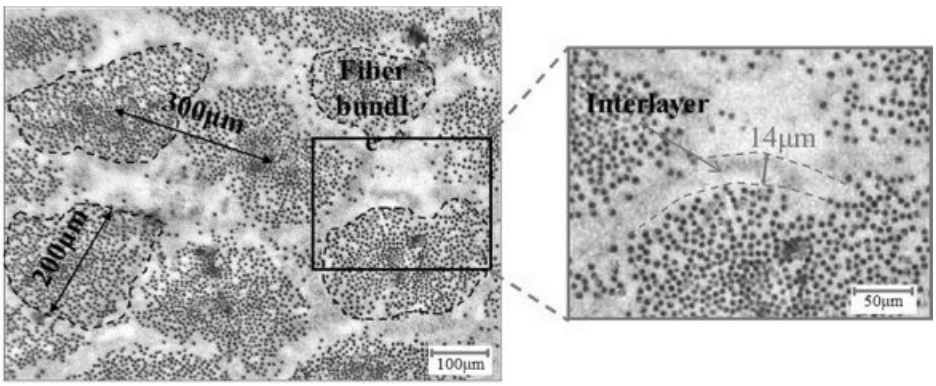

Fig. 2. Completed actual structure of self-healing fiber reinforced ceramics (by digital microscope).

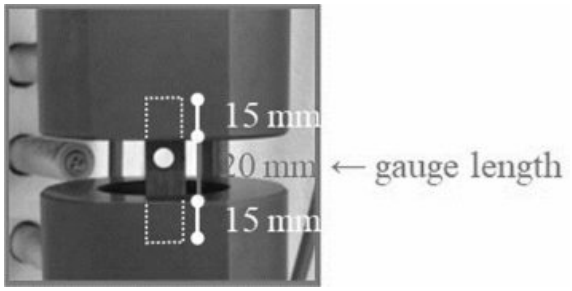

Fig. 3. Mounting of the test specimen.

concentration coefficient. The test apparatus used a universal testing machine (EHF-FB5KN, SHIMADZU CO., LTD., Japan) which can control a crosshead and a load by the lower hydraulic pump. The heating rate and the crosshead speed were set to 10ºC/minute and 10 N/second with reference to JIS R1723:2015 standard, respectively. The jig was manufactured using SiC having a relatively low thermal expansion rate even at high temperatures. The gauge length of the test specimen was 20 mm, and the strain was calculated to use the gauge length. The maximum stress was calculated by equations (2) and (3) considering stress concentrations.

$$\sigma_0 = \frac{P}{A} \quad (20$$

$$\sigma_{max} = \sigma_0 \alpha \quad (3)$$

Wherein A (mm^2) is the cross-sectional area, P (N) is the load, σ_0 (MPa) is the load per unit area, and σ_{max} (MPa) is the maximum normal stress to which the stress concentration factor is applied. The stress used in the test data was σ_{max} (MPa), and the cross-sectional area A was calculated by subtracting the diameter of the hole 4 mm since it was calculated in the region where stress concentration occurred. Fig. 3 shows the mounting of the specimen.

High temperature tensile test to determine creep stress conditions

A high temperature tensile test was performed to determine creep stress conditions. In the fiber reinforced composite ceramics, the internal structure was not uniform due to internal defects and voids during the compounding and sintering process. Thus, the average value of tensile failure stress was calculated by performing the tensile test three times [19, 20]. The temperature condition was set at 1,000 ºC, which is relatively slow, and 1,200 ºC, which is rapidly accelerating, considering the healing reaction rate of SiC at atmospheric pressure in the air [21]. The heating rate and the crosshead speed were 10 ºC/minute and 0.5 mm/minute, respectively, referring to the standards of JIS R 1687: 2009. The results of the high temperature tensile test are shown in Fig. 4. Tensile fracture stress at 1,000 ºC was 147.9 MPa, 197.6 MPa, and 156 MPa, respectively and the average fracture stress was 167 MPa. Tensile fracture stress at 1,200 ºC was 161.7 MPa, 143.2 MPa, and 142 MPa, respectively and the average fracture stress was 148 MPa. The temperature conditions of the high temperature creep test were determined by the average tensile stress. Creep stress conditions are 150 MPa, and 137 MPa respectively at 1,000 °C. and 137 MPa, 100 MPa, and 68.5 MPa, respectively at 1,200°C.

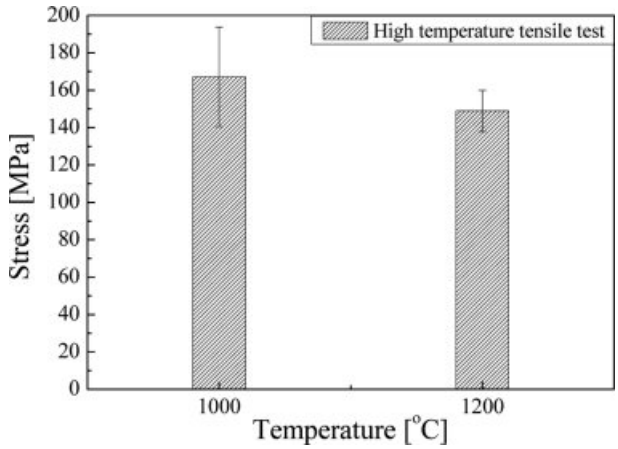

Fig. 4. High tensile strength at 1,000 ºC, and 1,200 ºC, respectively.

Results and Discussion

Effect of competition between damage and recovery on crack branching behavior

The creep test results at 1,000 ºC are shown in Fig. 5. Both creep rates converged to zero at the conditions of 150 MPa and 137 MPa, respectively. The creep rate converged to zero was 601 h at 150 MPa and 251 h at 137 MPa, respectively. From the fact that the creep rate converges to 0, it can be observed that the crack propagation is suppressed by the self-healing effect even though it is continuously damaged by the external force. Fig. 6 shows the observation of the surface before and after each test specimen. After the test of Fig. 6(a) and Fig. 6(b), the crack healed on the surface of the specimen was observed. The crack healing length in Fig. 6(a) was shorter than the crack healing length in Fig. 6(b). It can be observed that the crack propagation length depends on the stress and the crack healing length depends on the time when the creep rate converges to zero.

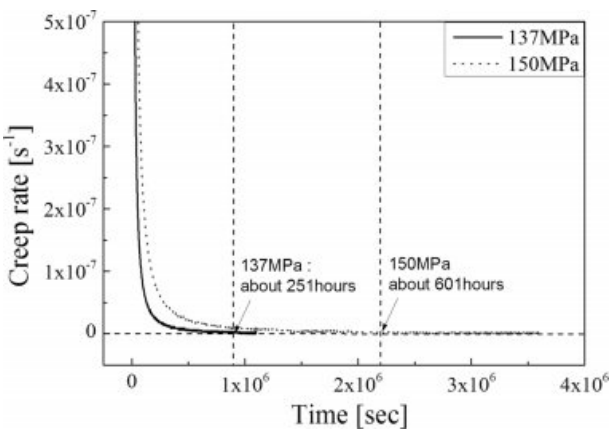

Fig. 5. Creep rate curve of the shFRC at 1,000 °C.

Strength recovery effect by self-healing

Ozaki et al. set the standard for self-healing that the strength of the healed part should be equal to or higher than the strength before the crack began [22]. Tensile tests were performed at room temperature on the specimens conducted at a stress of 137 MPa, and the results are shown in Fig. 7. Fig. 7(a) shows the stress rise section of the creep test and the stress-strain curve at room temperature tensile test. The crack initiation stress and strain increased. However, the slope after cracking was higher than that before the test. It is considered that this is because the crack branching at the weakest interface is made difficult by the self-healing reaction of the interface layer. Fig. 7(b) shows a photograph of the surface fractured by room temperature tension. The specimen was last fractured but no more cracks propagated at the healed crack part. This is because the interfacial layer designed with the weakest part designed was cured by high temperature oxidation in the process of healing the crack.

From the results in Fig. 7, it can be observed that the ductility is lowered and the fracture toughness and crack initiation stress are increased by interfacial curing. Additionally, the reduced strength after the initiation

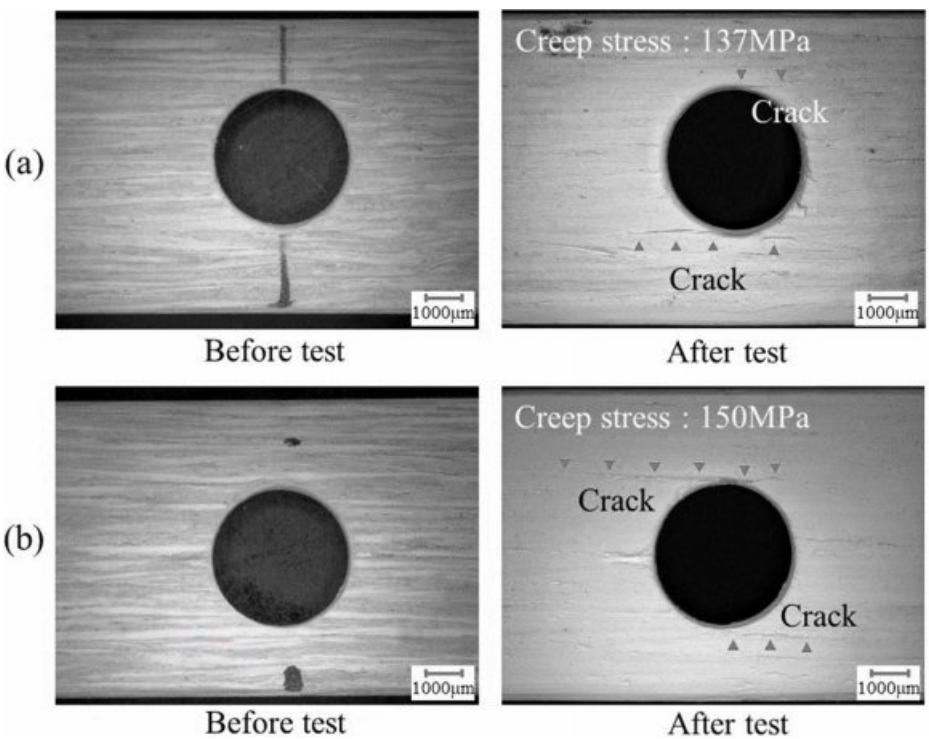

Fig. 6. Picture of specimen surface before and after the creep test (a) 137 MPa, (b) 150 MPa.

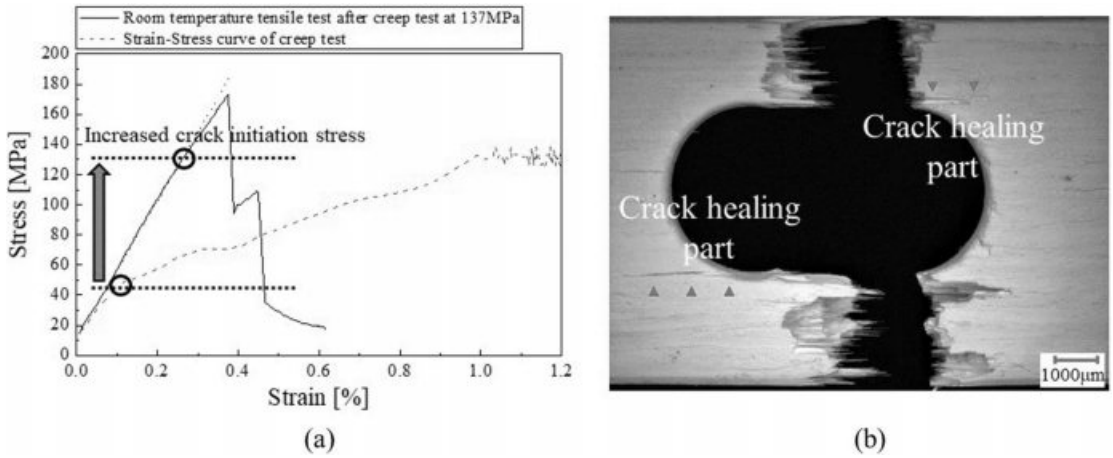

Fig. 7. (a) Comparative analysis of crack initiation stress before and after the creep test at 137 MPa, (b) Tensile fracture behavior observation after creep test.

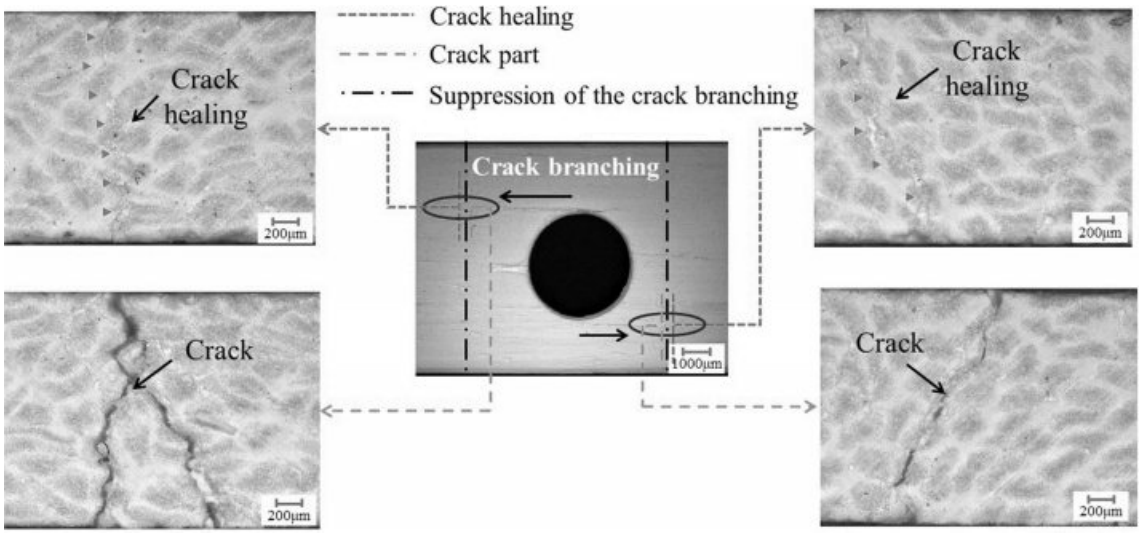

Fig. 8. Internal cross section of test specimen for 1,000 h at 1,000 °C, 150 MPa.

of the crack is recovered by self-healing, it was confirmed macroscopically that the crack no longer occurs in the healing part even when the fracture stress is loaded.

Fig. 8 shows an internal cross-sectional picture of stopped crack part after the high temperature creep test at 150 MPa. The part where the crack propagation stopped was confirmed macroscopically. It can be observed that at 150 MPa, the crack did not propagate again for 400 h after 601 h when the crack propagation stopped. In other words, it is suggested that the constant load stress at which the crack is stopped by self-healing can be designed to the allowable stress.

Effect of oxidation of interface layer on fracture behavior

Because of the hardening by oxidation of the interface layer, cracks become markedly difficult to propagate to the interface layer and most of the load is applied to the fibers. The creep tests were performed at 1,200 °C to investigate the influence of fracture behavior due to rapid oxidation of the interfacial layer. Fig. 9 shows creep curves at 68.5 MPa, 100 MPa, and 137 MPa, respectively. The fractured time at 100 MPa was 10.7 h, and the fractured time at 137 MPa was 246 seconds. In contrast, 68.5 MPa was not fractured for 1,000 h. Fig. 10 shows the time-creep rate curves for the creep tests conducted at 68.5 MPa. Fig. 10 shows the time-creep rate curves for the creep tests conducted at 68.5 MPa. Unlike the test results performed at 1,000 °C, the creep rate did not converge to zero for 1,000 h. However, it was confirmed that the creep rate continuously slowed. This is because interface hardening occurred by rapid oxidation before the crack propagated along the interface layer by the hardened interface.

Fig. 11 shows the surface photographs of before the test and after the test of the specimens performed at

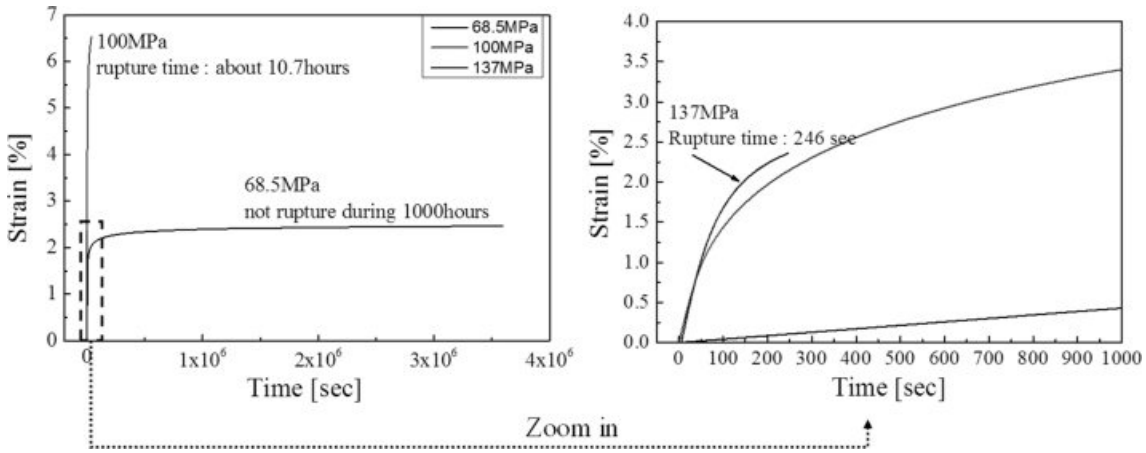

Fig. 9. Time-strain curve of the shFRC at 68.5 MPa, 100 MPa, and 137 MPa, respectively.

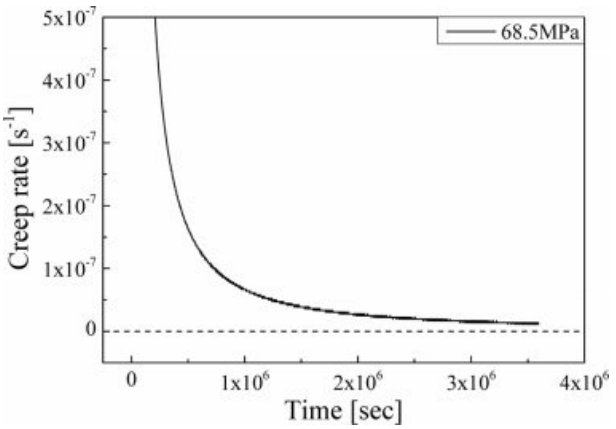

Fig. 10. Time-creep rate curve at 68.5 MPa, 1,000 h.

1,000 h 68.5 MPa. No crack was observed on the surface after the test, but it was confirmed that the hole was extended by approximately 0.2 mm in the load direction. The matrix exhibits Nabarro-Herring creep behavior in which atoms are diffused by prolonged high-temperature exposure at relatively low stress, and reinforcing fibers (γ-phase) are expected to drastically decrease in strength due to grain growth as the amorphous phase is transferred to the α-phase [23]. For this reason, it is thought that the fiber existing inside the test piece first fractured due to the decrease in strength of the fiber.

Fig. 12(a) and 12(b) show creep fracture surfaces of 137 MPa and 100 MPa, respectively. Fig. 12(c) shows the room temperature tensile fracture surface of a specimen subjected to creep test at 68.5 MPa for 1,000 h. It was confirmed that most of the interface layer was oxidized and the entire surface was white. Oriented fibers are not observed due to the thick oxide layer on the surface. This is because all of the SiC introduced into the interface layer was oxidized to SiO_2. And the pull-out length of the fiber is markedly short, and

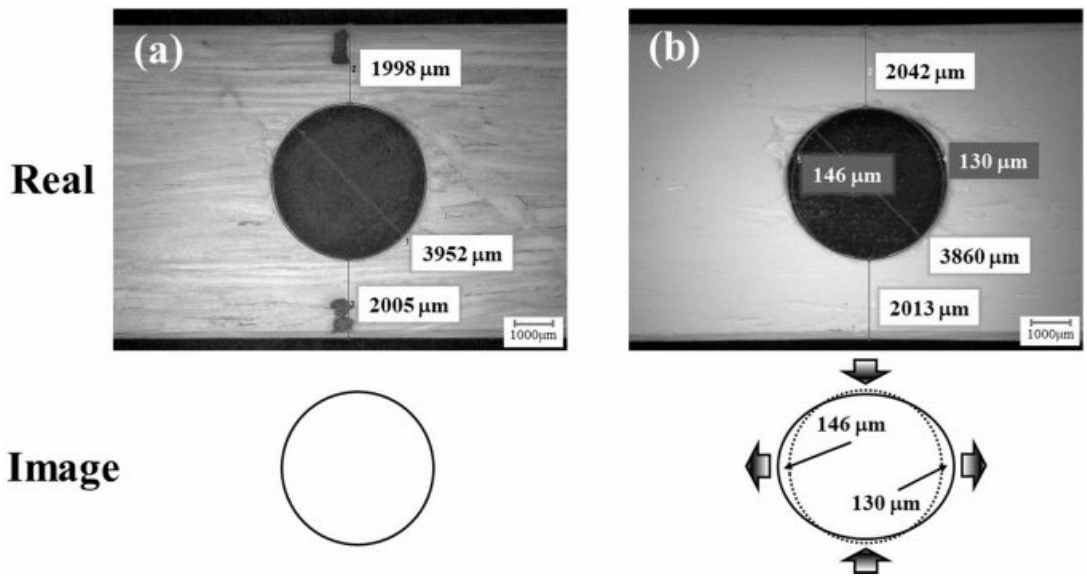

Fig. 11. Surface of the specimen of 68.5 MPa, 1,000 h condition (a) before the test (b) after the test.

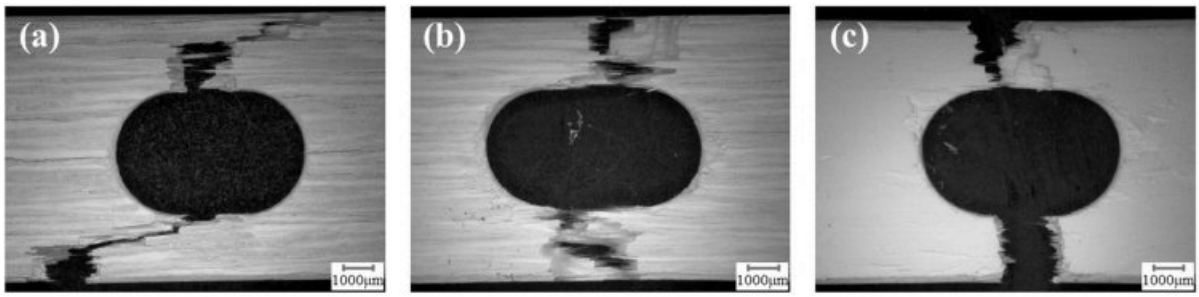

Fig. 12. Tensile fracture surface with stress condition (a) at 137 MPa, (b) at 100 MPa, (c) Tensile fracture surface of the specimen after the test at 68.5 MPa for 1,000 h.

almost no interface fracture occurs compared to Fig. 12(a) and Fig. 12(b). From the surface observation results, it has become clear that the above-mentioned decrease in strength of the fibers and the diffusion creep behavior of the base material appeared. Therefore, it is difficult to expect the delayed fracture by the fiber at 1,200 ºC.

Conclusion

In this study, we evaluated the crack propagation behavior when $Al_2O_3/SiC/Al_2O_{3f}$ damage and healing behavior occurred simultaneously. The results are as follow.

In the 1,000 ºC creep test, the time when the creep rate converged to zero was 601 h at 150 MPa and 251 h at 137 MPa, respectively. The higher the load stress, the longer the propagated crack length. Therefore, the crack propagation length of $Al_2O_3/SiC/Al_2O_{3f}$ depends on the stress and the crack healing length depends on the time when the creep rate converges to zero.

Since $Al_2O_3/SiC/Al_2O_{3f}$ makes it difficult to crack at the weakest interface layer by the self-healing reaction of the interface layer at 1,000 ºC, the fracture toughness and the crack initiation stress increases.

At 1,000ºC, when crack propagation is suppressed at a constant load and completely stops, cracks no longer propagates. Thus, it is suggested that creep stress higher than the crack initiation stress can be an allowable stress.

When the oxidation reaction rate of the interfacial layer is markedly rapid and the load stress is low (1,200 ºC, 68.5 MPa), the matrix shows diffusion creep behavior and the fiber shows a sharp decrease in strength due to phase transformation. And the interfacial layer makes it difficult for cracks propagation since all SiC is oxidized to SiO_2 before cracks are initiated. Thus, the fiber is first fracture inside. In this reason, it is difficult to expect a delayed fracture by fiber reinforcement.

At 1200 ºC, stopping and suppression of crack propagation is no observed, but at 1,000 ºC, a behavior is confirmed in which damage and healing occur simultaneously. Therefore, the suitable operating temperature of $Al_2O_3/SiC/Al_2O_{3f}$ is 1,000ºC.

Acknowledgement

This work has been supported by the Advanced Low Carbon Technology Research and Development Program (ALCA), JST, Japan.

References

1. L. Li, Mater Sci Eng, A, 695 (2017) 221-229.
2. L. Li, Compos B Eng, 66 (2014) 466-474.
3. N. Bansal and J. Lamon, Eds., in ”Ceramic Matrix Composites: Materials, Modeling, Technology, and Applications” (Wiley, 2013) p.217-234.
4. I.M. Low, Eds., in “Ceramic Matrix Composites: Microstructure, Properties and Applications” (Woodhead Publishing Limited, 2006) p.339-341.
5. H.H. Moeller, W.G. Long, A.J. Caputo, and R.A. Lowden, Ceram. Eng. Sci. Proc. 8 (1987) 977-984.
6. T. Fett, D. Munz, R.D. Geraghty, and K.W. White, Eng. Fract Mech 66 (2000) 375.
7. S. Kim, D.-Y. Yoo, and M.-J. Kim, Nemkumar Banthia, Cem. Concr. Compos. 104 (2019) 103335.
8. J.W.C. Pang and I.P. Bond, Compos. Sci. Technol. 65 (2005) 1791-1799.
9. C. Cluzel, E. Baranger, P. Ladevezèze, and A. Mouret, Composites, Part A 40[8] (2009) 976-984.
10. J. Lamon, in “Ceramic Matrix Composites: Materials, Modeling and Technology” (Wiley, 2014) p.40-64.
11. R.W. Rice, in Proceedings of the 5th Annual Conference on Composites and Advanced Ceramic Materials: Ceramic Engineering and Science Proceedings, Vol. 2, January 1981, edited by J.S. William (The American Ceramic Society, 1981) p. 661-701.
12. H. Li and H.X. Lu, S. Wang. Ceram. Int. 35 (2009) 901-904.
13. R. Bharthasaradhi and L.C Nehru. Phase Transitions. 89[1] (2016) 77-83.
14. K. Ando, T. Ikeda, S. Sato, F. Yao, and Y. Kobayasi, Fatigue Fract. Eng. Mater. Struct. 21 (1998) 119-122.
15. K. Ando, B.S. Kim, M.C. Chu, S. Saito, and K. Takahashi, Fatigue Fract. Eng. Mater. Struct. 27 (2004) 533-541.
16. W. Nakao, K. Takahashi, and K. Ando, Mater. Lett. 61 (2007) 2711-2713.
17. T. Osada, W. Nakao, K. Takahashi, and K. Ando, J. Am.

Ceram. Soc. 92 (2009) 864-869.
18. R.C.J. Howland, Trans. Roy. Soc. 229 (1930) 48-86.
19. W. König, Ch Wulf, P. Graß, and H. Willerscheid, Manuf. Technol. 34 (1985) 537-548.
20. R. Komanduri, Mach. Sci. Technol. 1 (1997) 113-152.
21. T. Osada, W. Nakao, and K. Ando, J. Am. Ceram. Soc. 92 (2009) 864-869.
22. S. Ozaki, T. Osada, and W. Nakao, Int. J. Solids Struct. 100-101 (2016) 307-318.
23. A.R. Bunsell and M.-H. Berger, in "Fine Ceramic Fibers" (Marcel Dekker, Inc., 1999).